Nanoscale

ROYAL SOCIETY OF CHEMISTRY

PAPER

View Article Online
View Journal | View Issue

Check for updates

Cite this: *Nanoscale*, 2025, **17**, 22905

Hot carrier transfer from $CsPbBr_3$ nanocrystals to Au_{25} clusters: the pivotal role of ligand-controlled diffusion

Shovon Chatterjee,[a] Arun Mukhopadhyay,[b,c] Surajit Mondal,[a] Smruti Sourav,[a] Suman Bhowmik,[d] Nirmal Goswami *[b,c] and Nimai Mishra *[a]

Received 15th May 2025,
Accepted 21st August 2025

DOI: 10.1039/d5nr02037a

rsc.li/nanoscale

Efficient hot carrier extraction from a lead halide perovskite is the key to overcoming its Shockley–Queisser limit. The interaction of the perovskite surface with an acceptor plays a vital role in controlling the charge transfer process. Here, we have investigated the charge transfer from $CsPbBr_3$ nanocrystals to Au_{25} clusters. Ultrafast pump–probe spectroscopy confirms that the Au_{25} cluster can efficiently extract hot carriers from the $CsPbBr_3$ nanocrystal. The effect of the ligand environment on the hot carrier transfer is studied by taking oleic acid/oleylamine (pristine) and trioctylphosphine-capped $CsPbBr_3$ nanocrystals of similar sizes. The experimental data show that the ligand-controlled diffusion mechanism governs the charge transfer process rather than anchoring. The hot carrier transfer process is found to be dependent on the effective interaction distance between the nanocrystal surface and Au_{25} controlled by the ligand environment. The hot carrier transfer rate to the Au_{25} cluster is estimated to be almost double for trioctylphosphine-capped $CsPbBr_3$ nanocrystals (9.53×10^{11} s^{-1}) compared to that of pristine nanocrystals (5.47×10^{11} s^{-1}). Thus, optimizing the ligand environment of the perovskite nanocrystals is essential for Au_{25} to harvest the hot carriers.

Published on 22 August 2025. Downloaded on 6/15/2026 2:27:59 AM.

1. Introduction

In the last decade, lead halide perovskite (LHP) nanocrystals (NCs) have emerged as promising materials for light harvesting and photocatalytic applications.[1,2] The defect-tolerant nature of these materials, with their large absorption cross-section and tunable band gap, makes them interesting candidates for the above-mentioned real-life applications.[2,3] In light-harvesting or photocatalytic applications, their charge carrier dynamics play an important role. The size, shape, and surface characteristics of NCs have a significant influence on their charge carrier dynamics.[4–7] The extraction of charge carriers from the NC surface is the predominant factor that controls their efficiency.[8] The extraction of band edge carriers is controlled by the thermodynamic feasibility of carrier transfer from the NC to the acceptor and most importantly by electronic coupling between the NC and the acceptor.[9] To achieve high optoelectronic and photocatalytic efficiency, extracting the hot carriers (HCs) from NCs is essential.[10] The HCs in LHPs are generated by photoexcitation with energy above the bandgap, and their carrier temperature is higher than their lattice temperature. These HCs then cool down as a result of the surplus energy being lost mostly through carrier–carrier and carrier–phonon scattering, which releases the energy as heat.[11] The efficient extraction of these HCs can overcome the Shockley–Queisser limit.[10]

However, the primary challenge of extracting these HCs is their fast decay on a sub-picosecond timescale to the band edge.[12] One of the primary directions of research to extract HCs focuses on slowing down the cooling process.[13] This HC cooling time can be tuned by control over NC size, dimensionality, trap states, and ligand engineering.[14–17] Critical parameters such as dielectric confinement, Auger heating, large polaron formation, hot phonon bottleneck, and high carrier densities have been revealed in these studies, which govern the physics of HCs. Over time, researchers have identified many acceptor molecules that can extract hot electrons or hot holes from LHPs, but still, efficient HC extraction remains a challenging task for the community.[12,18] Despite many accep-

[a]*Institute of Chemical Technology Mumbai, Indian Oil Odisha Campus Bhubaneswar, IIT Kharagpur Extension Center, Samantapuri Mouza, Gajapati Nagar, Bhubaneswar, Odisha 751013, India.*
E-mail: n.mishra@iocb.ictmumbai.edu.in
[b]*Materials Chemistry & Interfacial Engineering Department, CSIR-Institute of Minerals and Materials Technology, Bhubaneswar 751013, Odisha, India.*
E-mail: ngoswami@immt.res.in
[c]*Academy of Scientific and Innovative Research (AcSIR), Ghaziabad 201002, Uttar Pradesh, India*
[d]*Department of Chemistry, Indian Institute of Technology Kanpur, Kanpur-208016, India*

Published on 22 August 2025. Downloaded on 6/15/2026 2:27:59 AM.

tors having a band edge carrier extraction ability, very few of them have been found to be able to extract HCs before their cooling process. The mechanism behind the fast HC transfer process from the LHP to the acceptor is still elusive. Lim *et al.* identified the presence of an interfacial energy barrier that impedes the HC extraction process.[19] The interfacial electron–LO phonon coupling is the mechanistic pathway for HC transfer from $CsPbBr_3$ to Cs_4PbBr_6 in the $CsPbBr_3$@Cs_4PbBr_6 heterostructure proposed by Nie *et al.*[20] In a recent article, hot carrier transfer from $CsPbI_3$ to a fullerene has been proposed to go through the formation of a synergistic electronic state induced by effective interfacial bonding at the NC–fullerene junction.[21] The donor–acceptor interface plays a vital role in all these HC transfer processes. However, the low to moderate photostability issue of carbon-based nanomaterials like fullerenes makes them vulnerable under practical operating conditions.[22] Gold clusters are also found to be a good candidate for HC harvesting. Atomically precise gold nanoclusters have molecule-like discrete electronic structures that allow adjustable alignment with the donor valence or conduction band to optimize the carrier transfer processes.[23–26] Also, due to their very small size, gold clusters have a high surface area-to-volume ratio that should facilitate strong coupling with the $CsPbBr_3$ surface to enhance the charge transfer efficiency.[27,28] Also, these clusters show high photostability, making them a robust choice for applications.[29–31] The excited state electron transfer process was seen from $CsPbBr_3$ NCs to Au_{144} clusters through the formation of a $CsPbBr_3$–Au_{144} hybrid by Marjit *et al.*[18] The Au_{144} cluster was found to be an efficient hot electron acceptor. Au_{25} clusters have also been established as a good acceptor of electrons from CdSe nanoplatelets.[32] In these studies, the interfacial interaction between gold clusters and semiconducting nanocrystals plays a vital role in the charge transfer process and indicates that the gold clusters can act as an efficient HC acceptor. For the band edge carrier transfer process, acceptor binding to the NC surface also has a substantial role. Recently, Sarkar *et al.* showed the role of binding in the ultrafast hole transfer process.[33] DuBose *et al.* established how the ligand environment can affect the electron transfer process from $CsPbBr_3$ to methyl viologen by modulating the NC–acceptor interaction.[34] The charge transfer process from the LHP NC surface is mostly explained by the acceptor molecules' direct interaction with the NC surface. The through-space charge transfer in molecular systems is well known without the direct interaction of the donor and acceptor.[35,36] However, the charge transfer from the LHP NC surface to acceptor molecules without any direct interaction is rarely discussed. Sachith *et al.* reported a long-range diffusion-controlled electron transfer process from LHP NCs to C_{60} in the solution phase.[37] Ray *et al.* also showed that the donor–acceptor distance controlled by the thickness of encapsulating agents has a vital role in the charge transfer process.[38] In a recent article by Shah *et al.* the diffusion-controlled electron transfer process in the solution phase from LHP NCs to TiO_2 has been discussed, showing that shorter chain length ligands facilitate the excited state charge transfer process.[39] Although the aforementioned articles report the diffusion-controlled charge transfer process in PNC NCs, the role of ligand-controlled acceptor diffusion in the hot carrier transfer process is missing in the literature.

This study reports excited state carrier transfer from $CsPbBr_3$ NCs to Au_{25} clusters. In comparison with Au_{144}, Au_{25} clusters have more defined absorbance spectra in the UV-vis region and relatively more stability in solution.[40] Herein, the effect of the ligand environment on the carrier transfer process is investigated with oleic acid (OA)/oleylamine (OAm) capped (pristine) $CsPbBr_3$ NCs and amine-free trioctyl phosphine (TOP)-capped $CsPbBr_3$ NCs. In addition to having a shorter chain length than OA/OAm, which can reduce the ligand shell thickness, the TOP-capped amine-free $CsPbBr_3$ NCs have already been proven to exhibit superior stability compared to the amine-based ligand-capped NCs due to the absence of the dynamic nature of the ligand.[41] This also makes TOP-capped $CsPbBr_3$ NCs a better candidate for use in photocatalytic reactions to restrict their light-induced degradation. The Au_{25} clusters are found to be an excellent acceptor of HCs. From transient absorption spectroscopy, the HC transfer rate from TOP-capped $CsPbBr_3$ is calculated to be 9.53×10^{11} s^{-1}, almost double the HC transfer rate from pristine $CsPbBr_3$ NCs. From the steady state and time-resolved PL quenching of $CsPbBr_3$ NCs with Au_{25}, the presence of PL amplification due to the surface passivation of the clusters by the ligands has been identified, which suggests no direct binding of Au_{25} on the $CsPbBr_3$ surface, and the result is explained through a diffusion-controlled carrier transfer mechanism.

2. Results and discussion

The pristine and amine-free TOP-capped $CsPbBr_3$ NCs were synthesized through a modified hot injection procedure under open atmospheric conditions according to reported procedures.[41,42] The synthesis details are given in the SI (sections S1.2 to S1.4). The pristine $CsPbBr_3$ NCs are denoted as P-CPB, and the TOP-capped $CsPbBr_3$ NCs are denoted as AF-CPB. Both the NCs crystallize in the cubic crystalline phase (Fig. S1).[41,43] The NCs show broad absorption characteristics with the absorption band edge near 505 nm for P-CPB (Fig. 1a) and 507 nm for AF-CPB (Fig. 1b). P-CPB and AF-CPB also show bright PL with a sharp PL band centered at 513 nm (Fig. 1a) and 515 nm (Fig. 1b), respectively. The transmission electron microscopy (TEM) images of the synthesized P-CPB and AF-CPB are given in the insets of Fig. 1a and b, respectively. The detailed TEM characterization results are given in Fig. S2 and S3. The synthesized NCs have a square-shaped morphology (Fig. S2a and S3a). The average size of P-CPB is calculated to be 10.6 ± 2.4 nm (Fig. S2b), and for AF-CPB, it is found to be 11.4 ± 1.35 nm (Fig. S3b). The HRTEM images further confirm the cubic phase of the NCs (Fig. S2c and d for P-CPB and Fig. S3c and d for AF-CPB). P-CPB shows a PLQY of 61%, whereas AF-CPB exhibits a relatively higher PLQY of 85%, indi-

 This journal is © The Royal Society of Chemistry 2025

Published on 22 August 2025. Downloaded on 6/15/2026 2:27:59 AM.

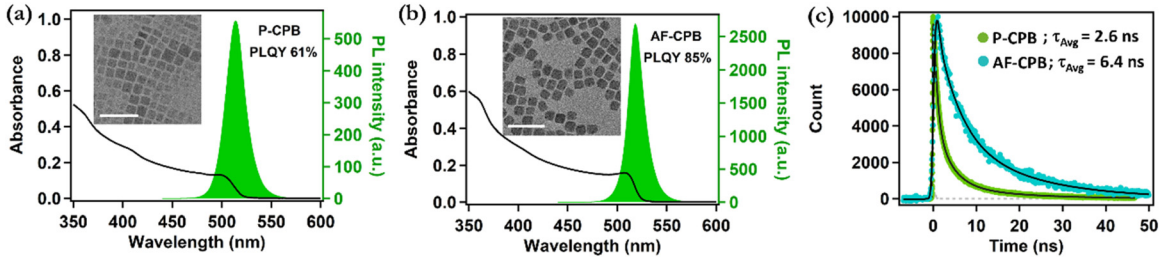

Fig. 1 Steady-state absorption and PL of the synthesized (a) P-CPB and (b) AF-CPB. The corresponding TEM images are given in the insets with a corresponding scale bar of 50 nm. (c) Time-resolved PL of P-CPB and AF-CPB.

cating less surface trap density. This also reflects on the time-resolved PL of the NCs (Fig. 1c). The PL transients of both P-CPB and AF-CPB were fitted with three exponential fitting parameters. AF-CPB shows an average PL lifetime of 6.4 ns, which is much longer than that of P-CPB, which exhibits an average PL lifetime of 2.6 ns. This longer PL lifetime of AF-CPB than P-CPB is associated with its lower surface trap density.[44]

Au_{25} clusters were prepared through the previously reported protocol by Zhu *et al.*[45] The detailed synthetic procedure is given in section S1.5 of the SI. The average size of the Au_{25} clusters is found to be ~1.7 ± 0.3 nm (Fig. S4). The Au_{25} clusters show a broad characteristic absorption feature with absorption peaks around 660 nm, 570 nm, and 440 nm, respectively (Fig. 2a). To evaluate the potential of Au_{25} clusters as electron/hole acceptors, cyclic voltametric (CV) measurements were carried out using a pure Au_{25} cluster suspension. The details of these measurements are provided in section S1.12 of the SI. The Au_{25} clusters show distinct reduction and oxidation peaks at −0.44 V and 0.74 V, respectively, in a Ag/AgCl electrode system. The exact positions of the reduction and oxidation peaks are extracted from the derivative plot (inset of Fig. 2b). From these oxidation and reduction potentials, the highest occupied molecular orbital (HOMO) and lowest occupied molecular orbital (LUMO) energy levels were calculated using the formulae[33]

$$E_{VB} = e(E_{ox} + 4.8 - E_{Fc/Fc^+}) \quad (1)$$

$$E_{CB} = e(E_{red} + 4.8 - E_{Fc/Fc^+}) \quad (2)$$

In the above two equations, E_{ox} and E_{red} refer to the oxidation onset potential and reduction onset potential, which are obtained from the cyclic voltammogram (Fig. 2b) and E_{Fc/Fc^+} (= 0.44 V) is the redox potential of ferrocene *vs.* SCE, taken from the literature.[33] The valence band (VB) and conduction band (CB) of CPB are −5.85 eV and −3.35 eV, also taken from the literature.[33] The HOMO and LUMO energy levels of the Au_{25} cluster are calculated to be −5.10 eV and −3.92 eV, schematically shown along with the energy levels of CPB in Fig. 2c. From the band position, it can be seen that both electron transfer and hole transfer are thermodynamically feasible from CPB to Au_{25} clusters. Another important factor is the possibility of energy transfer from CPB to Au_{25} clusters as the lower energy absorption bands of the clusters have an overlap with the PL spectrum of the CPB NCs. However, in a similar

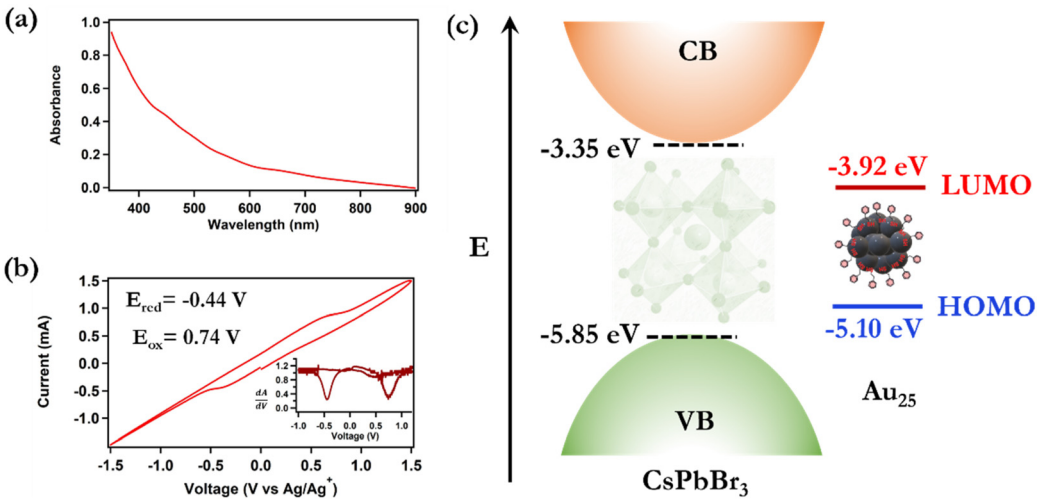

Fig. 2 (a) Absorption spectrum of Au_{25} clusters. (b) Cyclic voltammogram of the pure Au_{25} clusters at a scan rate of 10 mV s^{-1}. The corresponding derivative plot is given in the inset for estimating the exact oxidation and reduction peak potential. (c) Schematic energy level diagram of $CsPbBr_3$ NCs and Au_{25} clusters.

Published on 22 August 2025. Downloaded on 6/15/2026 2:27:59 AM.

scenario, the possibility of energy transfer from CPB to Au_{144} clusters was dismissed in the literature, due to inefficient spectral overlap.[18] Also, the Au_{25} clusters have a broad and weak PL spectrum with a maximum at 635 nm (Fig. S4c). The PL excitation (PLE) spectrum shows that the ground state involved in the origin of the PL is around 365 nm (Fig. S4c) and this state has no spectral overlap with the PL of CPB. So, the possibility of energy transfer to this state that can amplify the PL of Au_{25} is also nullified.

Following the band alignment of Au_{25} to CPB, the change in the PL intensity of both P-CPB and AF-CPB with varying concentrations of Au_{25} was monitored to observe the possible carrier transfer process. The experiment was done with a very low concentration of CPB NCs (~1.5 nM) to avoid the inner filter effect in the presence of a high ratio of Au_{25} clusters. The details of the CPB concentration calculation are given in section S1.13 of the SI. The Au_{25} cluster concentration was varied from 0 to 3.61 μM. The changes in PL intensity with the addition of Au_{25} of P-CPB and AF-CPB are given in Fig. 3a and b, respectively. As the Au_{25} cluster exhibits absorption in the excitation (400 nm) and PL regions (515 nm), the inner filter correction of the PL intensity is done (see section S14 of the SI). The corrected relative PL intensities are given in Table S1 and in the insets of Fig. 3a and b for P-CPB and AF-CPB, respectively. The expectation was to observe the quenching of PL intensity with the addition of the Au_{25} clusters. Surprisingly, at the early stage of the Au_{25} cluster addition (up to ~1 μM), we observed an amplification in the PL intensity for both P-CPB (inset of Fig. 3a) and AF-CPB (inset of Fig. 3b). A similar scenario was also observed by Shah *et al.* during the interaction of $CsPbCl_3$ NCs with $CuInS_2$, and this is explained by the passivation of surface defects by $CuInS_2$ quantum dots.[46] Following the PL amplification, we observed PL quenching for both P-CPB and AF-CPB at higher concentrations of Au_{25} clusters (Fig. 3a and b, respectively). This result indicates that in the overall scenario, two competitive processes are present that lead to this unusual PL behavior of the CPB NCs in the presence of varying concentrations of Au_{25} clusters. The possibility of ground-state interaction due to the change in PL intensity is ruled out by the additive nature of the absorption spectra of both P-CPB (Fig. S5a) and AF-CPB (Fig. S5b) in the presence of Au_{25} clusters. The TEM images of P-CPB and AF-CPB after the Au_{25} addition also show no morphological change in the CPB shape (Fig. S6a and S6d). Also, the Au_{25} clusters are found not to form any complex with the CPB NCs; rather, they are found separately around the NCs (Fig. S6a, b, d and e). The size histograms of P-CPB and AF-CPB after Au_{25} addition show average sizes of 11.05 ± 2.4 nm and 11.9 ± 1.2 nm, respectively, indicating no significant change in average size distribution in the system (Fig. S6c

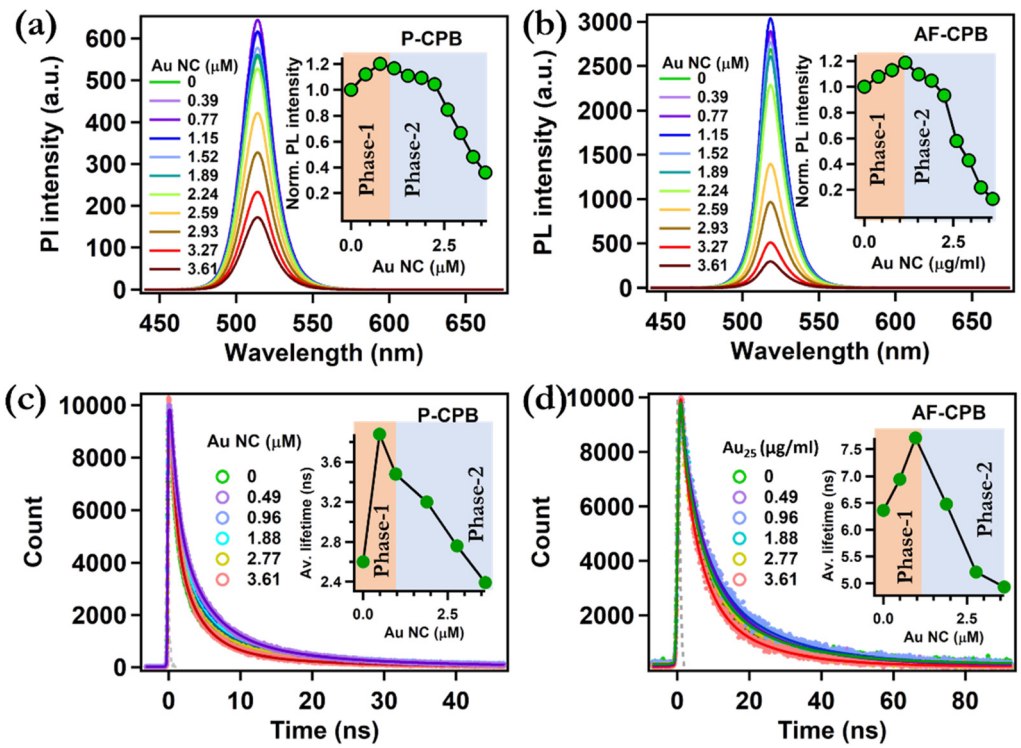

Fig. 3 Change in the PL of (a) P-CPB (1.5 nM) and (b) AF-CPB (1.5 nM) after the addition of Au_{25} NCs with a concentration range from 0 to 3.61 μM. The changes in relative normalized PL intensities (inner-filter corrected) for both P-CPB and AF-CPB are given in the insets of (a) and (b), respectively. PL transients of (a) P-CPB (1.5 nM) and (b) AF-CPB (1.5 nM) after the addition of Au_{25} clusters with a concentration range from 0 to 3.61 μM. The changes in average PL lifetimes for both P-CPB and AF-CPB are given in the insets of (c) and (d), respectively. The excitation source is a 405 nm laser with an instrument response function (IRF) of 120 ps (represented by the dotted lines.

 This journal is © The Royal Society of Chemistry 2025

Published on 22 August 2025. Downloaded on 6/15/2026 2:27:59 AM.

and S6f). P-CPB shows 70% PL quenching, whereas AF-CPB shows 91% quenching from its highest PL intensity after the addition of the Au_{25} clusters (3.61 μM). This further indicates that the process responsible for this PL quenching of the CPB NCs is more profound in the case of AF-CPB.

To investigate the excited state interaction between CPB and Au_{25}, PL transients for both P-CPB and AF-CPB were collected in the presence of varying concentrations of Au_{25} (Fig. 3c and d, respectively). The trends observed in average PL lifetimes are similar to the respective PL intensities. Without the addition of Au_{25}, P-CPB shows an average PL lifetime of 2.6 ns. The lifetime increased to 3.9 ns in the presence of 0.48 μM Au_{25}. Following this increment in the average lifetime, the PL decay becomes faster upon further addition of Au_{25}. A similar phenomenon happened with AF-CPB, where we observed that the PL lifetime increased to 7.7 ns from its original PL lifetime of 6.4 ns, followed by a shortening of the lifetime upon further addition of Au_{25}. This suggests that the change in the PL intensity is directly associated with the excited state process. For P-CPB, the average PL lifetime in the presence of 3.61 μM Au_{25} decreases by ~39% (from 3.9 ns, the lifetime at 0.49 μM Au_{25} concentration decreases to 2.4 ns), whereas for AF-CPB, the change is estimated to be 37% (from 7.7 ns to 4.9 ns). The trend in the change in PL lifetime and its extent are very similar for P-CPB and AF-CPB. However, the extent of change in the steady-state PL intensity of AF-CPB is much more prominent than that of P-CPB.

The interaction between CPB and varying concentrations of Au_{25} indicates the presence of two competitive processes. In a lower concentration regime of Au_{25}, the process responsible for the PL enhancement through modulation of the trap density minimization is dominant (phase-1 in Fig. 3a–d). However, at higher concentrations of Au_{25}, the quenching phenomenon becomes the dominant factor (phase 2 in Fig. 3a–d). From the band position of Au_{25}, it is obvious that in phase-2, the quenching phenomenon is controlled by Au_{25} through a facile carrier transfer process. To encounter PL enhancement along with an increment in the PL lifetime, a controlled experiment was done by treating the CPB NCs with phenyl ethane thiol (PET), which was used as a ligand for Au_{25}. The result shows that PET enhances the PL intensity of the CPB NCs, indicating surface reconstruction through passivation of the trap states present on the NC surface (Fig. S7). Also, IR spectroscopic measurement with P-CPB was done to see the possibility of ligand exchange between oleic acid and PET in phase-1. However, P-CPB shows no characteristic carbonyl stretching, confirming that OA is not the predominant ligand in the system; rather, oleylammonium acts as the primary ligand (Fig. S8).[47] After the addition of Au_{25}, we observed no change in the persistent stretching frequencies, confirming no ligand exchange. This overall result indicates that the PET ligand from the Au_{25} system passivates the CPB NC surface in phase-1 to amplify the PL intensity by modulating the trap density. This phenomenon may be a possible reason behind the PL amplification of both P-CPB and AF-CPB in phase-1. However, after the passivation of trap states present on the CPB surface, the PET cannot further amplify the PL intensity, and the quenching of PL by the Au_{25} becomes the dominant factor (phase-2). The overall proposed process is schematically shown in Scheme 1.

Therefore, it is clear from the steady state and time-resolved PL measurements that in the CPB–Au_{25} interaction, the Au_{25} clusters guide the quenching, while the surface passivation through PET guides the PL amplification. Also, the extent of quenching is higher in the case of AF-CPB than in P-CPB. Another key point is the disparity in quenching between steady-state and time-resolved PL measurements. The steady-state measurements show that the extent of PL intensity quenching is much more profound than the shortening of PL lifetime for both P-CPB and AF-CPB. As we have already discarded the ground state interaction between CPB and Au_{25} from the additive nature of the absorption spectrum, there must be an additional excited state process affecting this disparity.

To understand the origin of the PL quenching, we performed femtosecond transient absorption spectroscopy. The NCs were excited above the band gap at 400 nm using a femtosecond pulsed laser. For all the measurements, the exciton occupancy per pulse is calculated to be 2.32 and 2.87 for P-CPB and AF-CPB, respectively, indicating the possibility of a

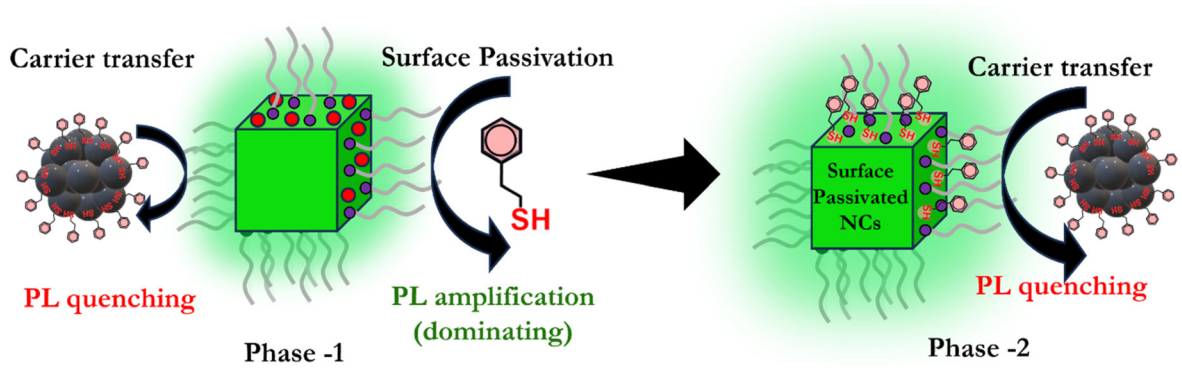

Scheme 1 Schematic illustrating the change in PL intensity upon the addition of Au_{25} clusters in CPB NCs (Fig. 3).

Published on 22 August 2025. Downloaded on 6/15/2026 2:27:59 AM.

multiexciton process involved (see S1.12 of the SI). Following excitation, a strong negative ground state bleach (GSB) signal is observed near the band edge position for both P-CPB and AF-CPB (Fig. S7a and S7b, respectively). This signal arises from the excitonic state-filling effect of hot carriers.[48] At an early time, a photoinduced absorption feature arises at ~520–570 nm for both the NCs due to the band gap renormalization process (Fig. S9a and S9b).[49] The derivative-like spectral feature at an early time originates from the coulombic interaction between hot excitons and probe pulse-induced band edge excitons.[48] This phenomenon is known as the biexciton-induced Stark effect, which is responsible for the redshift of the GSB signal at early delay times.[50] Following excitation in the early time delay regime, the GSB signals for both P-CPB and AF-CPB reach their peak intensities, indicating excitonic state filling by the relaxation of the HCs.[12] The HC cooling time is estimated to be 1590 fs for P-CPB and 850 fs for AF-CPB from the rise time of the GSB signal (Fig. S9c and Table S2). The hot carrier cools to the band edge through carrier–phonon interaction, and this cooling process is affected by several factors like size, shape, dimensionality, trap density, and ligands, as already discussed. Here for P-CPB and AF-CPB, the sizes are almost the same. The PLQY values suggest that AF-CPB has a lower trap density on its surface than P-CPB. So, if these traps are capable of trapping HCs, then the cooling time of P-CPB should have been faster than that of AF-CPB. But here we see exactly the opposite trend. So, the reason behind the faster cooling time in AF-CPB is not related to the trap density, and the ligand environment plays a crucial role in this process. Following the cooling of HCs, the time evolution of the TA spectra for P-CPB and AF-CPB is shown in Fig. S9d and S9e, respectively. The decay kinetics of the GSB is fitted with three exponential fitting equations (Fig. S9f and Table S2). The short time constant of ~45 ps predominantly originates from the biexciton recombination process.[51] However, as the trapping process also has a similar timescale, it can contribute to this short timescale. The time constant of ~250–350 ps originates from trion formation.[52] The longer decay component of >1.5 ns is due to the single exciton recombination process.[52] From the GSB decay kinetics, it is evident that AF-CPB shows slower decay kinetics than P-CPB (Fig. S9f). Notably, the short-time constant (~45 ps) has almost a 53% contribution to the overall decay kinetics of P-CPB, whereas for AF-CPB ~36% of the excited state population at the band edge relaxes through this process. This indicates that trapping in the decay dynamics of P-CPB may be the reason behind the higher contribution of the short-time constant.

To see the effect of Au_{25} on the CPB recombination dynamics, both P-CPB and AF-CPB NCs were studied in the presence of Au_{25}. For both the NCs, the NC to Au_{25} ratio was kept constant. The GSB decay dynamics of both P-CPB and AF-CPB remained almost unchanged in the presence of Au_{25} (Fig. 4a and b for P-CPB and AF-CPB, respectively). This may be because of the competitive surface passivation and band edge carrier transfer processes. However, interestingly, the amplitude of the GSB band at the time of completion of excitonic state filling decreases in the presence of Au_{25} for both P-CPB and AF-CPB (Fig. S10a and S10b, respectively). The decrease in this GSB amplitude signifies that not all the hot carriers formed upon 400 nm pulse excitation go to the band edge, but rather transfer to any other state. To understand this, the GSB formation dynamics of P-CPB and AF-CPB were monitored in the presence of Au_{25}. Earlier it was already mentioned that P-CPB and AF-CPB show a GSB formation time, *i.e.* the time taken for the HC cooling process of 1590 fs and 920 fs, respectively. In the presence of Au_{25}, the HC cooling of both P-CPB (850 fs) and AF-CPB (490 fs) becomes faster, indicating the HC transfer process from the CPB to Au_{25} clusters.

The bleach amplitude maximum is a direct measure of the number of carriers relaxing to the band edge that forms the GSB band. If the availability of the carriers that relax to the band edge becomes less, the amplitude gets reduced. Transferring HCs before the relaxation to the band edge thus directly reduces the GSB amplitude maximum.[12] Through the change in the absorption normalized bleach amplitude, we observe 21% HC transfer from P-CPB (Fig. 4e), whereas AF-CPB transfers almost 31% of its HCs to the Au_{25} NCs (Fig. 4f). So, the unavailability of the HCs for band edge exciton formation is one of the main reasons that reduces PL without affecting the PL lifetime. This HC transfer is the main reason behind the disparity of quenching extent observed through steady-state and time-resolved PL measurements.

Further from the difference in HC cooling times of CPB with and without Au_{25}, the HC transfer rate is calculated using the following equation;[12]

$$k(\text{hot CT}) = \frac{1}{\tau_{\text{CPB}-\text{Au}_{25}}} - \frac{1}{\tau_{\text{CPB}}} \quad (3)$$

where τ_{CPB} is the HC cooling time of the respective CPB NCs. $\tau_{\text{CPB–Au25}}$ is the HC cooling time of that particular CPB NC in the presence of Au_{25}. Using the above equation, the HC transfer rate is found to be 5.47×10^{11} s^{-1} for P-CPB and 9.53×10^{11} s^{-1} for AF-CPB. The HC transfer rate in AF-CPB is almost 1.8 times the HC transfer rate in P-CPB. From the steady state and time-resolved PL measurements, we also observed that the extent of quenching is greater in the AF-CPB system. So, from all the experimental evidence, it is evident that the hot carrier transfer process is more facile from AF-CPB than P-CPB (Scheme 2). The hot electron transfer rate from CPB to the Au_{144} cluster has been reported to be 1.05×10^{12} s^{-1}.[18] Also, the hot hole transfer from CPB to 4-mercaptophenol is estimated to be 2.3×10^{12} s^{-1}.[12] Although the hot carrier transfer rate from AF-CPB to Au_{25} is comparable to that reported in the literature, the rate is slow in the case of P-CPB. In our study, the hot carrier transfer rate is found to be on the slower side maybe because of the diffusion-controlled mechanism. As the Au_{25} cluster does not directly interact with the CPB surface, the coupling of the electronic states between CPB and Au_{25} becomes less efficient, which may retard the hot carrier transfer.

In general, for NCs, it has been reported that the interaction of the quencher with the surface of the NCs is necessary

 This journal is © The Royal Society of Chemistry 2025

Published on 22 August 2025. Downloaded on 6/15/2026 2:27:59 AM.

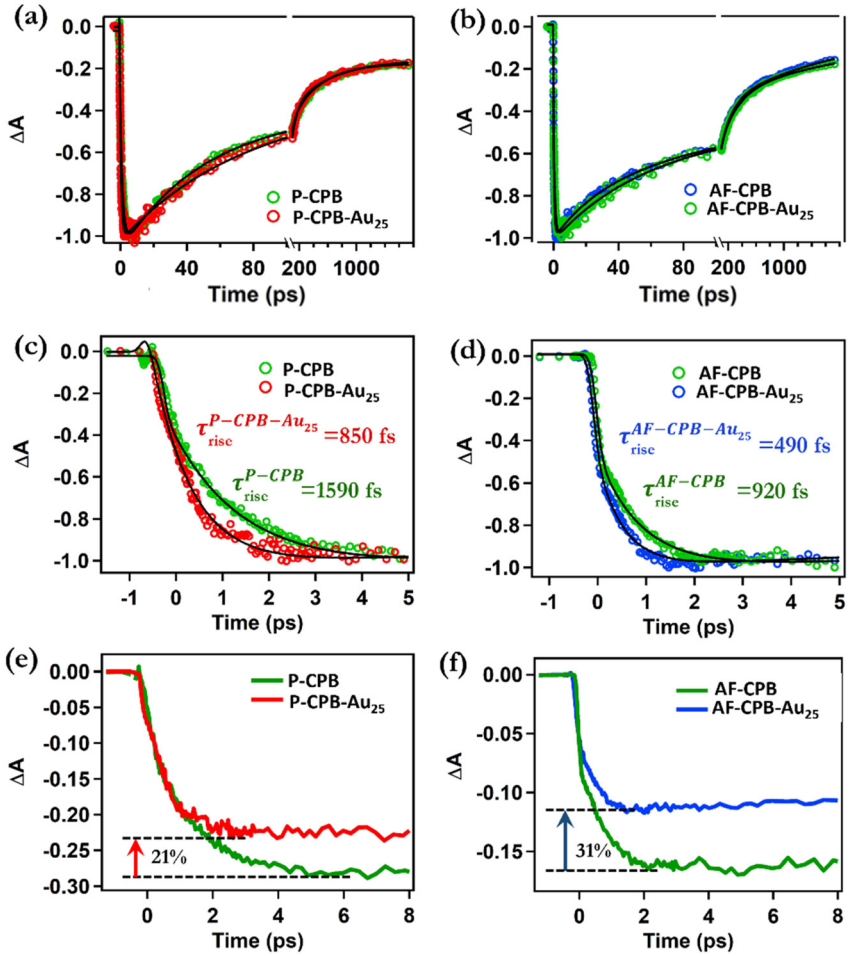

Fig. 4 The GSB bleach recovery kinetics of (a) P-CPB and (b) AF-CPB with and without Au_{25}. The hot carrier transfer process was observed from the growth dynamics of the GSB signals of P-CPB and AF-CPB when excited using a 400 nm laser pump. The comparable bleach formation kinetics of (c) P-CPB and P-CPB in the presence of Au_{25}, and (d) AF-CPB and AF-CPB in the presence of Au_{25}. The comparable bleach amplitudes of (e) P-CPB and P-CPB in the presence of Au_{25} and (f) AF-CPB and AF-CPB in the presence of Au_{25}.

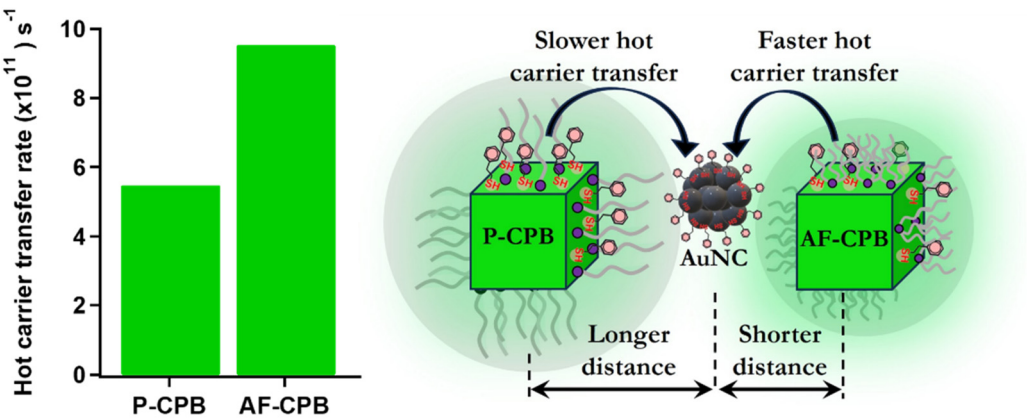

Scheme 2 Schematics showing the effect of distance controlled by the ligand environment on the diffusion-controlled hot carrier transfer process from P-CPB and AF-CPB to Au_{25}.

for the carrier transfer process. For perovskite NC systems, earlier reports suggest that the quencher binds to the NC surface before the carrier transfer process. Also, the electron transfer mechanism from $CsPbBr_3$ NCs to Au_{144} reported by Marjit *et al.* is based on the formation of a $CsPbBr_3$–Au_{144} hybrid structure.[18] The binding probability of the quencher to

Published on 22 August 2025. Downloaded on 6/15/2026 2:27:59 AM.

the NC surface is directly proportional to the binding energy and the available space on the NC surface. The available space on the NC surface is controlled through the trap density which is formed by ligand desorption. So, the bare surface should lead to a higher efficiency of binding, which helps better charge transfer. However, in our case, P-CPB has a higher trap density than AF-CPB. So, if the charge transfer process from CPB to Au_{25} occurs *via* direct surface interaction, then P-CPB should have a higher efficiency of quenching. In reality, we observe exactly the opposite trend for both band-edge carrier transfer and hot carrier transfer processes. Now, if the charge transfer process takes place without direct interaction with the NC surface, *i.e. via* a diffusion controlled mechanism, then the efficiency and rate of the charge transfer will be governed by the NC to quencher distance. For AF-CPB, TOP is an eight-carbon chain ligand, a much shorter ligand than OA/OAm. Thus, the permeability of the Au_{25} cluster to the CPB surface will be better for AF-CPB than P-CPB due to the effective shortening of the interaction distance, which leads to facile charge transfer from AF-CPB. So, from this argument and experimental observation, it is evident that both hot carrier and band edge carrier transfer processes from CPB to Au_{25} are diffusion-controlled and the ligand plays a vital role in controlling the rate of charge transfer.

3. Conclusions

In conclusion, we have studied the role of the ligand environment in the charge transfer process from CPB to Au_{25} clusters. P-CPB shows an overall 70% quenching of steady-state PL, while the quenching becomes more prominent in AF-CPB (91%) due to the short-chain length ligand environment. From the ultrafast transient absorption spectroscopic analysis, it has been found that Au_{25} clusters can efficiently extract hot carriers from the CPB NCs. The hot carrier transfer rate is found to almost double in AF-CPB (9.53×10^{11} s^{-1}) compared to that of P-CPB (5.47×10^{11} s^{-1}), indicating the strong influence of the ligand environment on the process. From all the experimental evidence, it has been shown that the charge transfer process does not go through anchoring; rather, it is guided by the ligand-controlled diffusion mechanism. The diffusion-controlled hot carrier transfer from perovskite NCs sets it apart as a compelling process, which, upon further investigation, could enable advanced applications in the areas of optoelectronics and energy conversion.

Conflicts of interest

The authors declare no competing financial interest.

Data availability

The data supporting the findings of this study are available from the corresponding author upon reasonable request. Supplementary information: materials, methods, synthetic procedures, and supporting data containing material characterization of NCs and clusters, and transient absorption spectra. See DOI: **https://doi.org/10.1039/d5nr02037a**.

Acknowledgements

This work is financially supported by the National Postdoctoral Fellowship (project number: PDF/2023/000211) and the Core Research Grant (CRG/2022/005380) from the Department of Science and Technology (DST)-Science and Engineering Research Board (SERB) of India. S. C. thanks the National Postdoctoral Fellowship (PDF/2023/000211) for providing postdoctoral fellowship support. A. M., S. M., and S. B. thank the UGC for providing graduate fellowship support. We sincerely acknowledge Prof. Pratik Sen of IIT Kanpur for helping with the transient absorption facility.

References

1 N. S. Peighambardoust, E. Sadeghi and U. Aydemir, *ACS Appl. Nano Mater.*, 2022, **5**, 14092–14132.
2 S. Chatterjee, S. Biswas, S. Sourav, J. Rath, S. Akhil and N. Mishra, *J. Phys. Chem. Lett.*, 2024, **15**, 10118–10137.
3 H. Huang, M. I. Bodnarchuk, S. V. Kershaw, M. V. Kovalenko and A. L. Rogach, *ACS Energy Lett.*, 2017, **2**, 2071–2083.
4 G. Ghosh, B. Jana, S. Sain, A. Ghosh and A. Patra, *Phys. Chem. Chem. Phys.*, 2019, **21**, 19318–19326.
5 S. B. Naghadeh, B. Luo, Y.-C. Pu, Z. Schwartz, W. R. Hollingsworth, S. A. Lindley, A. S. Brewer, A. L. Ayzner and J. Z. Zhang, *J. Phys. Chem. C*, 2019, **123**, 4610–4619.
6 F. Gabelloni, F. Biccari, G. Andreotti, D. Balestri, S. Checcucci, A. Milanesi, N. Calisi, S. Caporali and A. Vinattieri, *Opt. Mater. Express*, 2017, **7**, 4367.
7 S. Sourav, S. Mondal, S. Chatterjee, S. Biswas and N. Mishra, *Cryst. Growth Des.*, 2024, **24**, 6230–6237.
8 Y. Sheng, A. Zhao, L. Yu, S. Yuan, Y. Di, C. Liu, L. Dong and Z. Gan, *Phys. Status Solidi*, 2020, **257**, 2000198.
9 X. Chen, P. V. Kamat, C. Janáky and G. F. Samu, *ACS Energy Lett.*, 2024, **9**, 3187–3203.
10 W. Lin, S. E. Canton, K. Zheng and T. Pullerits, *ACS Energy Lett.*, 2024, **9**, 298–307.
11 J. Fu, Q. Xu, G. Han, B. Wu, C. H. A. Huan, M. L. Leek and T. C. Sum, *Nat. Commun.*, 2017, **8**, 1300.
12 A. De, S. Das and A. Samanta, *ACS Energy Lett.*, 2020, **5**, 2246–2252.
13 A. Das, K. Marjit, S. Ghosh, D. Ghosh and A. Patra, *J. Phys. Chem. C*, 2023, **127**, 15385–15394.
14 B. Yu, L. Chen, Z. Qu, C. Zhang, Z. Qin, X. Wang and M. Xiao, *J. Phys. Chem. Lett.*, 2021, **12**, 238–244.
15 A. Mahata, E. Mosconi, D. Meggiolaro, S. Fantacci and F. De Angelis, *Adv. Energy Mater.*, 2025, **15**, 2303405.

This journal is © The Royal Society of Chemistry 2025

Published on 22 August 2025. Downloaded on 6/15/2026 2:27:59 AM.

16 J. Ye, N. Mondal, B. P. Carwithen, Y. Zhang, L. Dai, X.-B. Fan, J. Mao, Z. Cui, P. Ghosh, C. Otero-Martínez, L. van Turnhout, Y.-T. Huang, Z. Yu, Z. Chen, N. C. Greenham, S. D. Stranks, L. Polavarapu, A. Bakulin, A. Rao and R. L. Z. Hoye, *Nat. Commun.*, 2024, **15**, 8120.
17 P. Zeng, X. Ren, L. Wei, H. Zhao, X. Liu, X. Zhang, Y. Xu, L. Yan, K. Boldt, T. A. Smith and M. Liu, *Angew. Chem., Int. Ed.*, 2022, **61**, e202111443.
18 K. Marjit, G. Ghosh, S. Ghosh, D. Ghosh, A. Medda and A. Patra, *ACS Phys. Chem. Au*, 2023, **3**, 348–357.
19 S. S. Lim, D. Giovanni, Q. Zhang, A. Solanki, N. F. Jamaludin, J. W. M. Lim, N. Mathews, S. Mhaisalkar, M. S. Pshenichnikov and T. C. Sum, *Sci. Adv.*, 2019, **5**, eaax3620.
20 Z. Nie, X. Gao, Y. Ren, S. Xia, Y. Wang, Y. Shi, J. Zhao and Y. Wang, *Nano Lett.*, 2020, **20**, 4610–4617.
21 Y. Li, J. Jiang, D. Wang, D. Liu, S. Yajima, H. Li, A. Fuchimoto, H. Li, G. Shi, S. Hayase, S. Tao, J. Shi, Q. Meng, C. Ding and Q. Shen, *Adv. Funct. Mater.*, 2025, **35**, 2415735.
22 N. Y. Doumon, M. V. Dryzhov, F. V. Houard, V. M. Le Corre, A. R. Chatri, P. Christodoulis and L. J. A. Koster, *ACS Appl. Mater. Interfaces*, 2019, **11**, 8310–8318.
23 I. Chakraborty and T. Pradeep, *Chem. Rev.*, 2017, **117**, 8208–8271.
24 Y. Du, C. Li, Y. Dai, H. Yin and M. Zhu, *Nanoscale Horiz.*, 2024, **9**, 1262–1278.
25 L. Chen, M. Gharib, Y. Zeng, S. Roy, C. K. Nandi and I. Chakraborty, *Mater. Today Chem.*, 2023, **29**, 101460.
26 L. Zeng, M. Zhou and R. Jin, *ChemPhysChem*, 2024, **25**, e202300687.
27 H. Qian, M. Zhu, Z. Wu and R. Jin, *Acc. Chem. Res.*, 2012, **45**, 1470–1479.
28 S. R. Sahoo, T. K. Dinda, S. Saha, P. Mal and N. Goswami, *ACS Appl. Mater. Interfaces*, 2025, **17**, 19669–19681.
29 S. Zhou, B. Peng, Y. Duan, K. Liu, O. Ikkala and R. H. A. Ras, *Angew. Chem., Int. Ed.*, 2022, **61**, e202210808.
30 J. A. de Jong, M. S. Workentin and M. Hesari, *ChemPhotoChem*, 2025, **9**, e202400236.
31 Nonappa, *Beilstein J. Nanotechnol.*, 2020, **11**, 533–546.
32 A. Medda, A. Dutta, D. Bain, M. K. Mohanta, A. De Sarkar and A. Patra, *J. Phys. Chem. C*, 2020, **124**, 19793–19801.
33 P. Sarkar, A. Sen, A. Dutta, R. Kumar and P. Sen, *J. Phys. Chem. C*, 2025, **129**, 1252–1259.
34 J. T. DuBose and P. V. Kamat, *J. Phys. Chem. C*, 2020, **124**, 12990–12998.
35 P. Mukherjee, A. Das, A. Sengupta and P. Sen, *J. Phys. Chem. B*, 2017, **121**, 1610–1622.
36 S. Ghosh, S. K. Mondal, K. Sahu and K. Bhattacharyya, *J. Phys. Chem. A*, 2006, **110**, 13139–13144.
37 B. M. Sachith, T. Okamoto, S. Ghimire, T. Umeyama, Y. Takano, H. Imahori and V. Biju, *J. Phys. Chem. Lett.*, 2021, **12**, 8644–8651.
38 S. Ray, M. R. Sahoo, S. Mukherjee, A. Perumal, S. K. Nayak and S. Bhaumik, *RSC Adv.*, 2023, **13**, 35551–35561.
39 S. A. B. Shah, S. Ghimire, R. Lesyuk, M. V. Diamanti, V. Lughi and C. Klinke, *Small Sci.*, 2024, **4**, 2300348.
40 X. Yuan, N. Goswami, I. Mathews, Y. Yu and J. Xie, *Nano Res.*, 2015, **8**, 3488–3495.
41 S. Akhil, M. Palabathuni, S. Biswas, R. Singh and N. Mishra, *ACS Appl. Nano Mater.*, 2022, **5**, 13561–13572.
42 S. Samanta, S. Paul and T. Debnath, *Small*, 2024, **20**, 2311712.
43 M. S. Kirschner, B. T. Diroll, P. Guo, S. M. Harvey, W. Helweh, N. C. Flanders, A. Brumberg, N. E. Watkins, A. A. Leonard, A. M. Evans, M. R. Wasielewski, W. R. Dichtel, X. Zhang, L. X. Chen and R. D. Schaller, *Nat. Commun.*, 2019, **10**, 504.
44 S. Akhil, V. G. V. Dutt, R. Singh and N. Mishra, *J. Phys. Chem. C*, 2022, **126**, 10742–10751.
45 M. Zhu, E. Lanni, N. Garg, M. E. Bier and R. Jin, *J. Am. Chem. Soc.*, 2008, **130**, 1138–1139.
46 S. H. Shah and T. Debnath, *J. Phys. Chem. Lett.*, 2024, **15**, 2580–2586.
47 N. Fiuza-Maneiro, K. Sun, I. López-Fernández, S. Gómez-Graña, P. Müller-Buschbaum and L. Polavarapu, *ACS Energy Lett.*, 2023, **8**, 1152–1191.
48 K. J. Babu, G. Kaur, A. Shukla, R. Saha, A. Kaur, M. Sachdeva, D. K. Yadav and H. N. Ghosh, *ACS Photonics*, 2022, **9**, 969–978.
49 V. Kumar, V. Nagal, R. Kumar, S. Srivastava, B. K. Gupta, M. Kumar, A. K. Hafiz and K. Singh, *RSC Adv.*, 2020, **10**, 34651–34657.
50 J. Aneesh, A. Swarnkar, V. K. Ravi, R. Sharma, A. Nag and K. V. Adarsh, *J. Phys. Chem. C*, 2017, **121**, 4734–4739.
51 S. Chatterjee, A. Sen and P. Sen, *Mater. Chem. Front.*, 2023, **7**, 753–764.
52 S. Nakahara, H. Tahara, G. Yumoto, T. Kawawaki, M. Saruyama, R. Sato, T. Teranishi and Y. Kanemitsu, *J. Phys. Chem. C*, 2018, **122**, 22188–22193.